Applied Physics A (2023) 129:575
https://doi.org/10.1007/s00339-023-06854-0

Applied Physics A
Materials Science & Processing

Investigation of dual intrinsic a-Si:H films for crystalline silicon surface passivation by spectroscopic ellipsometry: application in silicon heterojunction solar cells

Ashutosh Pandey[1] · Shrestha Bhattacharya[1] · Jagannath Panigrahi[1] · Sourav Mandal[1] · Vamsi Krishna Komarala[1]

Received: 12 May 2023 / Accepted: 19 July 2023 / Published online: 26 July 2023

Abstract
The microstructure factor (R^*) of the PECVD-grown intrinsic amorphous silicon (i-a-Si:H) layer plays a crucial role in crystalline silicon (c-Si) surface passivation and charge carrier transport in silicon heterojunction (SHJ) solar cells. In this work, we have used stack of i-a-Si:H passivation layers deposited at two different temperatures to improve the c-Si surface passivation by minimizing the interface defect density at the a-Si/c-Si interface. The initial i_1-a-Si:H layer is deposited on the c-Si at ~ 150 °C with a high R^*, and the second i_2-a-Si:H layer is deposited at 230 °C with a low R^*. Ex-situ ellipsometry analysis of i-a-Si:H layers provided information related to the void fraction of the thin films due to modification in the Si–$H_{\geq 2}$ and Si–H bonding environment, which plays a vital role in atomic H migration towards i-a-Si:H/c-Si interface. Combining the low- and high-temperature i-a-Si:H layer stack enhanced the cell precursor passivation to ~ 2.1 ms with an implied V_{oc} of ~ 714 mV. Furthermore, implementing the optimized thickness (2 nm + 8 nm) of the i-a-Si:H stack (with 40% void fraction in i_1-a-Si:H layer) in the device has led to the power conversion efficiency of ~ 19.06%.

Keywords Intrinsic amorphous silicon · Surface passivation · Bilayer · Ellipsometry · Heterojunction · Silicon solar cell

1 Introduction

In silicon heterojunction (SHJ) solar cells, reducing charge carrier recombination at the front and rear surfaces of c-Si has been a critical process step in obtaining high power conversion efficiencies [1, 2]. A few nanometers of thin intrinsic hydrogenated amorphous silicon (i-a-Si:H) film deposited by low-temperature PECVD process provides excellent passivation of the crystalline silicon (c-Si) surfaces [3]. In the last few years, the approach to the i-a-Si:H passivation layer employed in the SHJ cell has evolved dramatically, that is, from the device-grade single amorphous silicon layer to bilayer or multilayer passivation [4–7], and discussed in more detail in a recent review [8].

Earlier, the general recipe for obtaining high-level a-Si:H/c-Si interface passivation was depositing the amorphous layer close to the amorphous-to-microcrystalline transition regime [9, 10] and performing subsequent post-deposition annealing. To avoid unwanted epitaxial growth at the a-Si/c-Si interface, deposition parameters such as RF power density, pressure, hydrogen dilution, and temperature of the i-a-Si:H layer must be chosen wisely. It has been demonstrated that a highly depleted silane plasma is beneficial for the growth of the transition zone i-a-Si:H films and for refraining from epitaxy formation at the interface [10]. A post- or intermediate-step brief hydrogen plasma treatment (HPT) procedure is also significant in improving the passivation quality of the i-a-Si:H layer [11]. The substrate temperature also decides the deposited film's microstructural properties and the a-Si:H/c-Si interface passivation quality [12]. The effect of deposition temperature on the growth of a high-quality single passivation layer and its impact on SHJ device performance parameters has been reported by Ruan et al. [13] and recently by Zhao et al. [14]. The growth at very low temperatures results in micro-voids-rich amorphous films [15, 16] and sometimes polysilane formation in the chamber [17, 18]. High-temperature deposition or high hydrogen dilution of SiH_4 often leads to the formation of epitaxial silicon [15].

✉ Vamsi Krishna Komarala
vamsi@iitd.ac.in

[1] Solar Photovoltaics Laboratory, Department of Energy Science and Engineering, Indian Institute of Technology Delhi, New Delhi 110016, India

An approach to completely avoid the formation of an epitaxial layer at the a-Si:H/c-Si interface is to deposit the i-a-Si:H layer with a high microstructure factor R^*, also called the under-dense or porous layer. This layer should be optimized to maintain the implied V_{oc} same, which usually reduces after the subsequent doped layer deposition [19]. The porous layer with a high R^* is often realized in a pure SiH_4 plasma at high power and pressure conditions. The benefit of this effect was soon discovered in an innovative bilayer passivation concept. Sai et al. [4, 20] have shown the beneficial use of a bilayer passivation approach consisting of the porous i-a-Si:H layer (adjacent to the c-Si) having a high R^* value and a dense i-a-Si:H overlayer (deposited on the first layer) in terms of interface passivation improved by ~ fourfold, and SHJ device efficiency has enhanced by about ~ 1.8%. Furthermore, Luderer et al. [6] have extended the work, showing a bilayer structure with an i_1 layer deposited using pure silane condition as a porous interfacial layer with a dense i_2 layer, and investigated the trade-off between interface passivation and charge carrier transport, which has led to the series resistance reduction followed by an increase in fill factor, and with overall improvement in power conversion efficiency with respect to their baseline. Moreover, different researchers used various deposition temperatures to fabricate high-efficiency cells with a single i-a-Si:H layer; still, the microstructure effect and the passivation quality of the interface are not investigated.

In this work, we have explored the i-a-Si:H bilayers for the c-Si surface passivation and further applied in SHJ solar cell fabrication, wherein the two layers with different R^* are realized using a different approach, i.e., deposition temperature variation. The microstructure has been investigated systematically using spectroscopic ellipsometry and is found to be dependent on the deposition temperature of the i-a-Si:H layer. In this two-step deposition, the i-layer adjacent to the silicon surface (i_1-a-Si:H) is deposited at a low temperature (LT), and the capping i-layer (i_2-a-Si:H layer) is made at a higher temperature (HT). The dielectric function, the hydrogen bonding of the i-a-Si:H layer, and the silicon surface passivation of the layers made at different temperatures are individually characterized. Furthermore, the initial i_1-a-Si:H layer thickness optimization in the stack with an i_2-a-Si:H layer is also investigated for cell precursor passivation (just before ITO deposition), and the SHJ solar cell performance.

2 Experimental details

As-cut phosphorous-doped n-type FZ c-Si (100) wafers (~ 250 µm thick, 1–3 Ω.cm) having a bulk lifetime of ~ 2.5 ms were used for the investigation. After the conventional precleaning step in piranha solution for 10 min to remove organic contaminants, the as-cut wafers were textured using 2 wt.% potassium silicate solution and 6 v/v.% IPA as an additive at 75–80 °C for 50 min to generate a random pyramidal surface with < 111 > orientation. The average pyramid size was measured as 3–5 µm [21]. The textured wafers were processed for wet chemical cleaning steps such as RCA 1 and RCA 2 using NH_4OH, HCl, H_2O_2, and HF. Intrinsic and doped amorphous silicon layers were deposited by a capacitively coupled plasma-enhanced chemical vapor deposition (PECVD reactor chamber volume of ~ 15 L) system equipped with a 13.56 MHz frequency generator as a plasma excitation source from the Excel Instruments. The intrinsic amorphous silicon layers were deposited using SiH_4 and H_2 gas mixture in a fixed dilution ratio and flow rate, which we optimized earlier [22]. The schematic diagram of the SHJ cell and detailed deposition conditions of the i-a-Si:H layers are summarized in Fig. 1 and Table 1, respectively. At first, keeping the other parameters fixed, the deposition temperature varied from 120 °C to 260 °C to study the change in structural properties of the i-a-Si:H layers and c-Si surface passivation. For comparison, SHJ devices were initially fabricated with two different i-a-Si:H layers

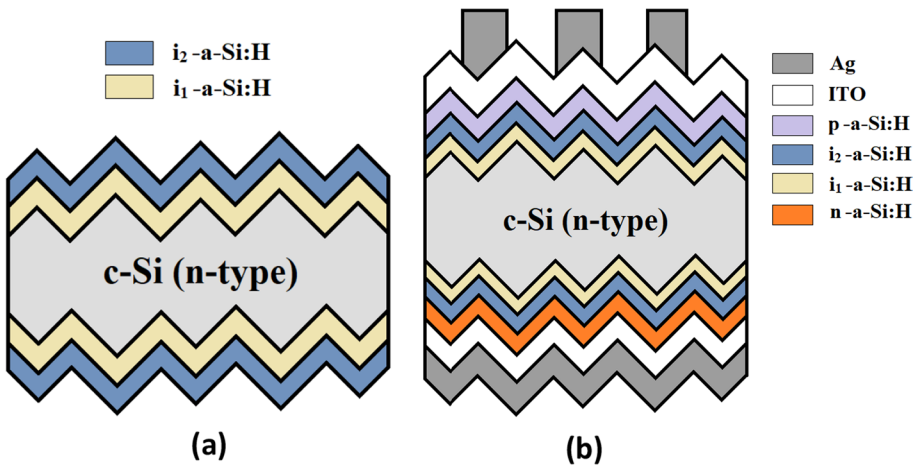

Fig. 1 Schematics of the **a** cross-sectional view of the c-Si surface passivation test structure, and **b** front junction SHJ solar cell investigated in this study

Table 1 Detailed deposition conditions for the i_1-a-Si:H and i_2-a-Si:H passivation layers

Deposition parameters	i_1-a-Si:H layer	i_2-a-Si:H layer
Electrode spacing (mm)	20	
Flow rate SiH_4/H_2 (sccm)	30/30	
Power Density (mW/cm^2)	44	
Deposition Pressure (Torr)	1	
Substrate Temperature (°C)	150 (LT)	230 (HT)

deposited at 150 °C and 230 °C temperatures keeping other deposition parameters similar. A symmetric heterostructure of the type i-a-Si:H (~ 10 nm)/c-Si/i-a-Si:H (~ 10 nm) was prepared on the textured silicon wafer for the passivation study. The passivation quality in terms of effective minority carrier lifetime (MCL), and implied open-circuit voltage (iV_{oc}) was measured by the Sinton WCT-120TS lifetime tester. The i-a-Si:H thickness measurements were performed on single-side polished plain silicon wafers using variable angle spectroscopy ellipsometry (VASE) (J.A. Woollam, M-2000, USA). The amorphous nature and void fraction validation in (~ 10 nm) i-a-Si:H layer and its optical parameters were extracted and analyzed by fitting the raw VASE data using the Tauc–Lorentz and Bruggeman effective medium approximation (BEMA) models. The microstructure and hydrogen bonding state information was obtained from the FTIR measurement (Thermo-Fisher Nicolet iS50) setup performed with i-a-Si:H layer deposited on the single side polished wafer.

The FTIR measurement used to extract the microstructure factor (R^*) using the formula:

$$R^* = I_{HSM}/I_{HSM} + I_{LSM} \quad (1)$$

where LSM and HSM stand for the low-frequency stretching mode (from 1980 to 2010 cm^{-1}) and high-frequency stretching mode (from 2070 to 2100 cm^{-1}), respectively [23–25], I is the integrated absorbance [24]:

$$I = \int \frac{\alpha}{\omega} d\omega \quad (2)$$

where α is the absorption coefficient, ω is the frequency in cm^{-1}, and α is proportional to $-\ln[T(\omega)]/t$ if $\alpha(\omega)t << 1$. $T(\omega)$ is the transmittance obtained from the FTIR measurements, and $'t'$ is the effective thickness of the films obtained from ellipsometry analysis.

After that, a two-step deposition temperature was adopted to optimize the i-a-Si:H passivation layer on both sides of the textured silicon wafer. The initial i_1-a-Si:H layer is deposited at a low temperature (150 °C) named LT, followed by the second i_2-a-Si:H layer deposited at a relatively high temperature (230 °C) named HT. The total thickness of the i-a-Si:H layer was fixed at ~ 10 nm by varying the individual thickness of each layer. Phosphine (4% in SiH_4) and diborane (3% in H_2) were as dopant gases for n^+-a-Si:H and p^+-a-Si:H deposition as electron- and hole-selective layers in SHJ solar cell. Indium tin oxide (ITO) of ~ 70 nm thickness was used as front and rear transparent conductive oxide (TCO) layers in the device structure. ITO layers were deposited at 120 °C substrate temperature via reactive sputtering with process pressure maintained at 4×10^{-3} Torr and a power density of 1.5 Wcm^{-2}. The target used for ITO deposition has the composition of In_2O_3:SnO_2 (90:10 wt.%), 20 sccm Ar and 0.06 sccm O_2 was used as reactive gases for both the front and rear side layers. The electrical properties of 70 nm deposited ITO film were measured using a Hall measurement setup from the Ecopia HMS-3000 system. It has mobility of ~ 31 cm^2/V-s, a bulk carrier concentration of ~ 3.66×10^{20} cm^{-3}, and a resistivity of 5.38×10^{-4} Ω-cm. Finally, thermally evaporated Ag (~ 1 µm) formed the busbar and fingers using a metal mask used as a front contact, and the backside was fully metalized using the same material. The area of the fabricated SHJ solar cell was 1.7×1.7 cm^2 with ~ 7% front metal grid coverage. Series resistance-free pseudo-fill factor (pFF) was measured using the *Suns-Voc* setup from the Sinton WCT-120TS instruments. To evaluate the SHJ device power conversion efficiency, light J–V characteristics were measured using the Class AAA solar simulator (Oriel Sol3A) using a xenon lamp at STC, i.e., cell temperature of 25 °C and an irradiance of 100 mW/cm^2 with an AM 1.5G spectrum.

3 Results and discussion

3.1 Effect of the deposition temperature of i-a-Si:H layers on c-Si surface passivation

Figure 2 shows the influence of substrate temperature (T_{sub}) on the effective minority carrier lifetime (MCL) measured on the as-deposited symmetric ~ 10 nm i-a-Si:H passivated samples at an excess carrier density of 1×10^{15} cm^{-3}. The figure shows that the passivation quality of the as-deposited films is poor at low T_{sub}, i.e., ≤ 150 °C. Therefore, the amorphous silicon films grown at low temperatures are unable to saturate the dangling bonds on the c-Si surface effectively. Afterwards, the MCL of the sample improved with the temperature and reached ~ 1130 µs with the T_{sub} of 230 °C, indicating improvement in interface passivation. With further increase in T_{sub} the lifetime value dropped to ~ 397 µs, indicating that the interface quality deteriorates at deposition temperatures > 230 °C. Therefore, the amorphous silicon films' deposition temperature significantly impacts the silicon surface passivation. The a-Si:H/c-Si interface passivation quality has been related to the tendency of the

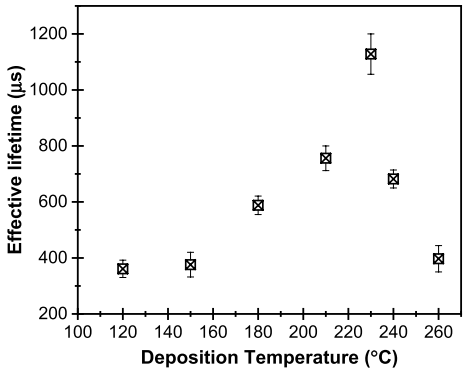

Fig. 2 Substrate temperature-dependent effective minority carrier lifetimes of c-Si wafers after ~ 10 nm symmetric i-a-Si:H passivation layers

growing amorphous films to relax the a-Si:H/c-Si interface by the growth of epitaxial silicon at a higher temperature, which deteriorates the passivation quality [15]. Schulze et al. [16] have reported that the interface defect density (D_{it}) and hydrogen content (C_H) increase with a decrease in T_{sub}, and the changes in the interface passivation quality have been ascribed to the defect equilibration between the a-Si:H bulk and the a-Si:H/c-Si interface. Therefore, a link exists between an a-Si:H bulk defect density (N_d) and the substrate temperature [26]. The N_d usually exhibits a U-shaped characteristic with respect to T_{sub}; at low T_{sub}, N_d is high because of the lower diffusivity of the SiH_3 radicals on the substrate surface and poor H mobility, and as a result, a large number of defects (weak bonds) are frozen into the network. As the T_{sub} increases, the SiH_3 diffusivity and H mobility enhance, thereby saturating the dangling bonds and a minimum N_d is noticed in the intermediate T_{sub}. At higher T_{sub}, enhanced H-mobility (or spontaneous H desorption at sufficiently high T_{sub}) and thermal disorder again lead to higher defect density in the film. As the bulk a-Si:H defect density equilibrates with the a-Si:H/c-Si interface states density during the PECVD, an equivalent T_{sub} dependence of the interface passivation quality can be expected.

To examine the microstructural properties of the a-Si:H films and any interface epitaxy formation, we have analyzed the pseudo-dielectric function $<\varepsilon>$ of the film/substrate structure obtained from the ellipsometric data. The $<\varepsilon_2>$ spectrum of the bare c-Si surface has two characteristic peaks at the critical points E_1 (3.4 eV) and E_2 (4.3 eV); the peaks are intense and have maximum values of > 30 and > 40, respectively. Figure 3a shows the $<\varepsilon_2>$ spectra of the ~ 10 nm i-layers deposited on the c-Si at different temperatures. It is clear that, at all temperatures, the $<\varepsilon_2>$ spectra deviate significantly from characteristic transition peak values of pristine c-Si, meaning that the films are amorphous, and no sign of epitaxy is seen at higher

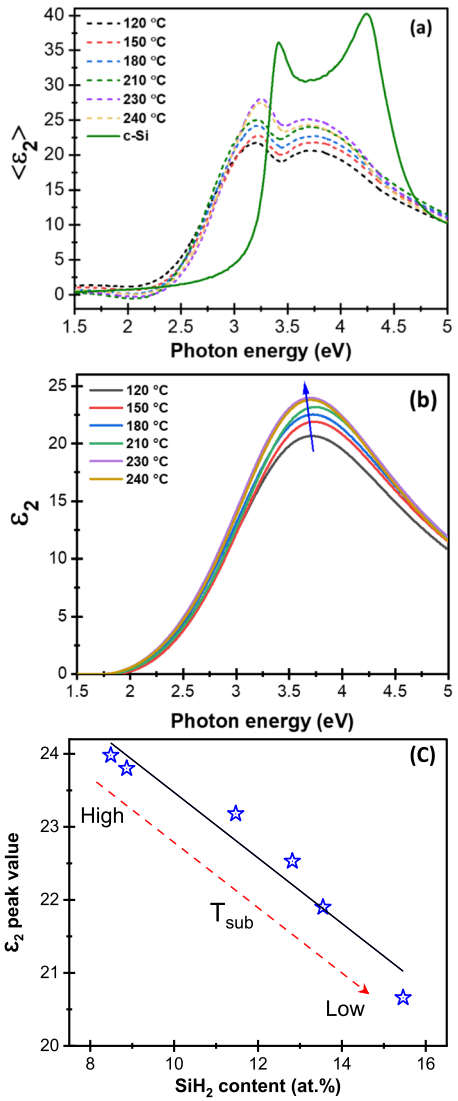

Fig. 3 **a** Imaginary part of the pseudo-dielectric $<\varepsilon_2>$ spectra of the i-a-Si:H films on the c-Si with different substrate temperatures, c-Si wafer spectrum also shown for reference, **b** variation in the ε_2 spectra of the as-deposited thin a-Si:H layers deposited at different substrate temperatures. **c** Peak values of ε_2 (star symbols) are plotted as a function of the $Si–H_2$ content estimated from FTIR spectra analysis in the a-Si:H layers (arrow shows from high to low substrate temperature deposition)

deposition temperature. Furthermore, from the variation of the ε_2 spectra of the a-Si:H films (Fig. 3b), it is observed that there is a gradual increase in the peak amplitude with an increase in the T_{sub}. It is also known that ε_2 represents the fundamental light absorption within a-Si:H, thus, symbolizing the film density. However, the film density does not improve above 230 °C, a slightly lower peak value of ε_2 is found at 240 °C. The amplitude or peak value of ε_2 also correlates well with the $Si–H_2$ bond density, plotted in Fig. 3c. There is a quite linear reduction in the ε_2 peak value with an

increase in the Si–H_2 content. The Si–H_2 content estimated from FTIR spectroscopy measurement rises from 8.49% to 15.46% (shown in Fig. 3c) as T_{sub} decreases, indicating an increase in the Si–H_2 bonded hydrogen content in the film. High Si–H_2 content suggests the presence of microvoids in the a-Si:H network, whereas the dense amorphous network mainly comprises the Si–H bonding configuration [27]. Hence, based on the ε_2 spectra and Si–H_2 bond density, it seems that a void-rich film is formed at low T_{sub}, and dense films are obtained at higher T_{sub}. The Si–H_2 bonds, although hydrogen-rich, do not mediate in c-Si/a-Si:H interface passivation unless annealed [15, 16], as they are preferably located around the microvoids [27]. Therefore, the a-Si:H/c-Si interface passivation quality deteriorates at low T_{sub} and increases with an increase in T_{sub}. At a temperature beyond 240 °C, the lifetime value lowers. A similar temperature dependence of surface passivation has been observed earlier, but the lowering in surface passivation at the higher T_{sub} was assigned to the film epitaxy [28]. However, in our films, epitaxy is not indicated in the $<\varepsilon_2>$ spectra based on the experimental parameters. Therefore, the lower passivation quality at a higher T_{sub} of 240 °C can be attributed to the induced changes in the amorphous film quality, probably due to the activation of secondary gas phase reactions at this higher temperature and excessive hydrogen extraction from the film. Matsuda [25] highlighted that the reactive radicals formed in the plasma may undergo secondary reactions, as given below with the precursor gasses SiH_4 and H_2 in the reaction chamber, which can be speculated for hydrogen molecule recombination and abstraction:

$$SiH_2 + H_2 \rightarrow SiH_4 (\text{Reaction related to recombination}) \quad (3)$$

$$H + SiH_4 \rightarrow H_2 + SiH_3 (\text{Reaction related to abstraction}) \quad (4)$$

The influence of T_{sub} on the i-a-Si:H layers is investigated for the optical bandgap, and deposition rate variation using the ellipsometry analysis, and the total hydrogen content (C_H), and microstructure factor (R^*) using the FTIR spectroscopy. Figure 4 summarizes the obtained parameters of the i-a-Si:H layers as a function of T_{sub}. There is a monotonic decrease in deposition rate with an increase in T_{sub} (Fig. 4a), which can be explained based on the temperature dependence of the diffusion of the silyl (SiH_x) radicals on the film-growing surface. The initial film growth consists of three different processes in the reaction chamber: (i) dissociation of SiH_4 into SiH_x radicals, (ii) transport of the generated radicals to the film-growing surface, and (iii) surface reactions (based on its reactivity, temperature, and pressure) between the generated radicals and the c-Si substrate. In our case, since the dissociation conditions are fixed, we expect the variation in film quality to be due to the change in the SiH_x diffusion and hydrogen mobility at the growing surface. At the low temperature, surface diffusion of silyl radicals (SiH_x) is low, and the probability of condensation is high, resulting in a higher deposition rate with a highly disordered film. With an increase in T_{sub}, enough activation energy is available to promote H abstraction and saturation of the dangling bond sites with SiH_3 allowing compact and dense film growth.

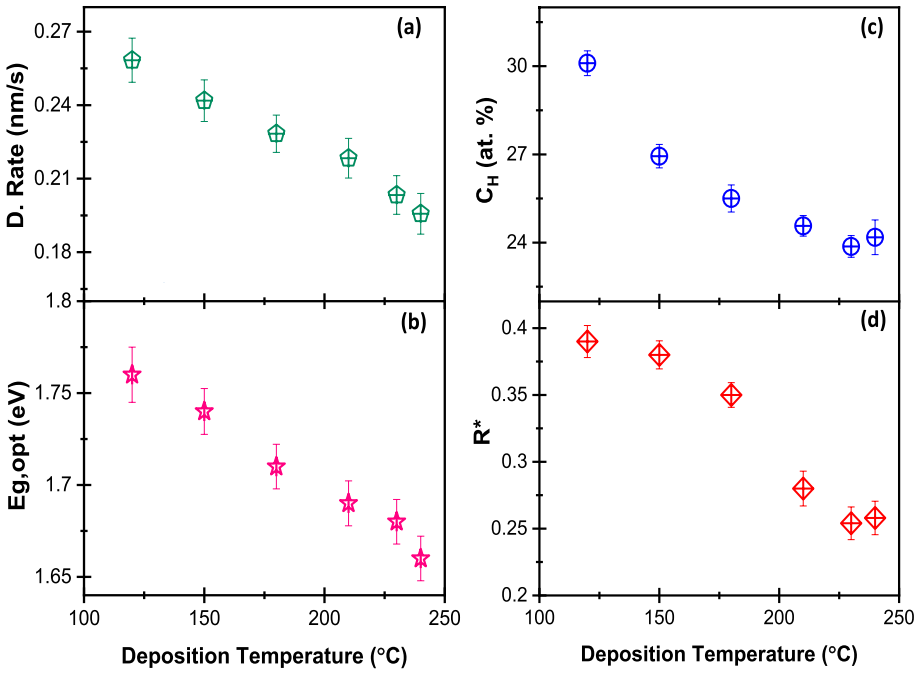

Fig. 4 Variation in **a** deposition rate, and **b** optical bandgap estimated from the ellipsometry analysis, **c** total hydrogen content (C_H), and **d** microstructure factor (R^*) from FTIR spectra analysis with the substrate temperature

The optical bandgap ($E_{g,\mathrm{opt}}$) decreases from 1.76 to 1.67 eV with an increase in T_{sub} from 120 °C to 240 °C, as shown in Fig. 4b. The total C_H content of the a-Si:H films also decreased similar to an increase in temperature (Fig. 4c). The enhancement in hydrogen mobility with increased temperature explains the gradual decrease in the total C_H content and the energy bandgap $E_{g,\mathrm{opt}}$. With an increase in the total C_H, the a-Si:H valence band edge moves down in energy, widening the energy bandgap [29]. The gradual decrease in the total bonded hydrogen content (C_H) with an increase in temperature can be due to a reduction of the amount of hydrogen-bonded as poly-hydride $(SiH_2)_n$, which makes the film more compact in nature and incorporation of fewer hydrogen atoms can be expected. The R^* increases with the decrease in T_{sub} (Fig. 4d), indicating the formation of relatively porous film at lower temperatures and hence corresponds to the presence of a high density of interface defects. Whereas at high temperatures, low R^* of the films corresponds to the formation of a dense a-Si:H network resulting in better silicon surface passivation.

3.2 Influence of stacked i-a-Si:H layer on silicon surface passivation

In this section, we discuss the impact of the individual LT (150 °C) and HT (230 °C) layers of ~ 10 nm as well as the stack of LT and HT passivation layers each of ~ 5 nm on the c-Si surface passivation. In the previous section, we have observed that the low-temperature deposited i-a-Si:H layers have high Si–H_2 bonding with high R^*. Therefore, to have the porous interface layer in the stack passivation, the i_1-a-Si:H layer at 150 °C is directly deposited on the < 111 > c-Si surface, followed by a compact i_2-a-Si:H layer deposited at 230 °C. Figure 5 shows the effective minority carrier lifetime graphs of the symmetric (~ 10 nm) passivated samples as a function of the excess carrier density. It is seen that the dense HT i-a-Si:H layer enables comparably good surface passivation of silicon with an effective carrier lifetime of ~ 1 ms, whereas the LT porous layers result into poor c-Si surface passivation, giving a lifetime of only ~ 215 µs. However, the passivation level achieved for the single layer is insufficient; therefore, a stack of layers has been tried and found effective. Compared to the level of passivation by the individual LT and HT i-a-Si:H layers, the stack of LT and HT i-a-Si:H layers enable better c-Si surface passivation, the effective lifetime of c-Si reaching more than 1.3 ms.

To deduce the recombination parameters, especially the interface D_{it}, the measured lifetime data are modelled using the calculations based on the a-Si:H/c-Si dangling bonds (DBs) recombination models [30, 31]. The dashed line represents the calculated lifetimes due to intrinsic recombination ($\tau_{\mathrm{int},R}$) [32]. The dashed–dot line represents the

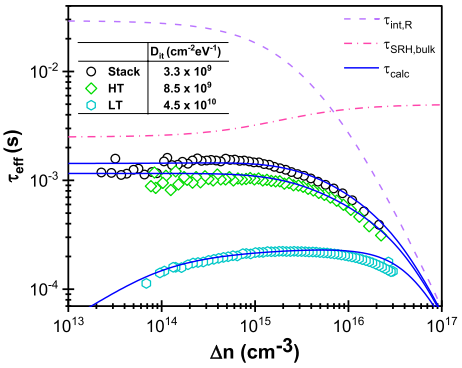

Fig. 5 Fitted effective minority carrier lifetime graphs of the passivated c-Si samples with ~ 10 nm i-a-S:H layer deposited at 150 °C (LT), and 230 °C (HT) and compared with a combination of 150 °C and 230 °C (stack) of equal thickness of ~ 5 nm. Symbols are experimental data, and the dashed, dashed dot, and continuous lines are related to calculated minority carrier lifetimes due to the intrinsic, bulk SRH, and contribution from intrinsic, bulk SRH, and surface recombination, respectively

estimated minority carrier lifetime due to the bulk SRH recombination ($\tau_{\mathrm{SRH,bulk}}$) using a bulk lifetime of 2.5 ms measured by quinhydrone solution [33]. The continuous line represents the calculated lifetime (τ_{calc}), the intrinsic, bulk SRH contribution, and the surface recombination contribution. The surface lifetime (τ_{surf}) is obtained from the a-Si:H/c-Si recombination model mainly by varying the D_{it} in the model; more details can be found in the reference [22]. For τ_{surf} calculation, an effective charge Q_{eff} accounts for both the amorphous layers and interface charges are taken. Considering the charge neutrality condition ($Q_{\mathrm{Si}} + Q_{\mathrm{eff}} = 0$) and band bending at the c-Si/a-Si:H interface, τ_{surf} is solved numerically using MATLAB program. Leendertz et al. [31], suggested that for the interface, the cross-sectional ratios of the DB states are set to be 1 and 10, respectively, for neutral (σ_n^0/σ_p^0) and charged (σ_n^+/σ_n^0 and σ_p^-/σ_p^0) states. The typical value of $\sigma_p = 1\times10^{-16}$ cm^2 and Q_{eff} value between 5×10^{10} and 10×10^{10} cm^2 are used.

The lowest D_{it} of 3.3×10^9 cm^{-2} eV^{-1} is obtained for the stack passivation sample. The LT passivation sample gave the maximum D_{it} of 4.55×10^{10} cm^{-2} eV^{-1}. Therefore, the a-Si:H deposited at low T_{sub} leaves a high density of unsaturated dangling bonds (DBs) at the interface as well as in the bulk of the layer. Whereas, in the stack, because of the presence of high Si–H_2 content in the interfacial LT layer, the i_2-a-Si:H layer deposition at a relatively high temperature (230 °C), makes these H atoms move around and passivate the unsaturated DBs, thereby further reducing the D_{it}. The surface recombination velocity (SRV) measures the rate at which excess carriers recombine at the c-Si/a-Si interface. Since we have used high-quality FZ silicon wafers having a bulk lifetime of 2.5 ms, the contribution from the bulk can be neglected. In such a case, $S_{\mathrm{eff}} = d^*(2\tau_{\mathrm{eff}})^{-1}$, where τ_{eff} is

the effective minority carrier lifetime and *'d'* is the wafer thickness (230 µm used in this work). The S_{eff} values are 57.2 cm/s and 11.27 cm/s for the LT and HT passivation, respectively. The S_{eff} value is further reduced to 7.8 cm/s as we employed the stack of these two i-a-Si:H layers. The lifetime results clearly demonstrate and support using the i-a-Si:H layer stack to effectively saturate the DBs at the a-Si:H/c-Si interface.

Figure 6 shows the absorption coefficient spectra obtained from the FTIR analysis of the deconvoluted i-a-Si:H films from 1850 to 2200 cm^{-1}. The spectra are fitted with two Gaussian functions that peaked at 2000 cm^{-1} (Low stretching mode—LSM) and 2100 cm^{-1} (High stretching mode—HSM), representing Si–H and Si–H_2 stretching modes, respectively. At 150 °C, the absorption by HSM is relatively high compared to the 230 °C condition, which indicates that the i-a-Si:H film contains more hydrogen in the LT film, becomes microvoid rich, and has many structural defects. These results correlate with the ellipsometry's $<\varepsilon 2>$ analysis in the previous section. In the HT i_2-a-Si:H layer, the HSM percentage in the absorption is lower compared to its LT counterpart, showing that i-a-Si:H film grown at high temperatures contains fewer microvoids and is relatively dense in nature. The absorption coefficient of the stack indicates that both the LSM and HSM contents in the i-a-Si:H film is higher, which means higher bonded hydrogen content in this layer. It was also observed that the overall hydrogen content (~ 32%) in the stack i-a-S:H layer is higher than the individual layers. This also confirms the lifetime measurement results in which the stack showed a higher level of c-Si surface passivation.

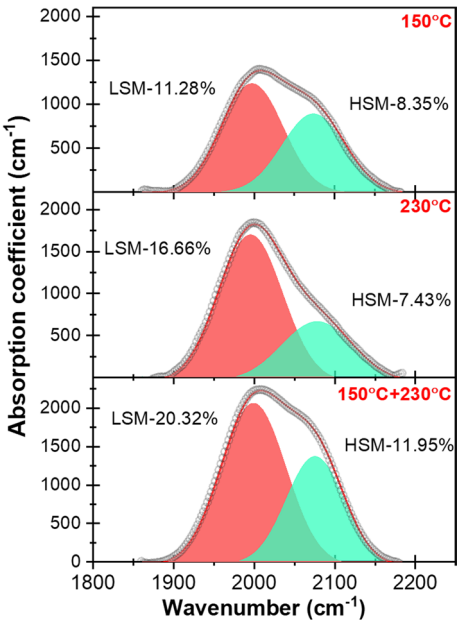

Fig. 6 Deposition temperature dependent Gaussian fitted FTIR absorption coefficient spectra of i-a-Si:H thin films deposited on the c-Si wafer

3.3 Optimization of porous LT i_1-a-Si:H layer characteristics

Figure 7a shows the variation in the imaginary part of the pseudo-dielectric function $<\varepsilon_2>$ of i_1-a-Si:H films were grown at 150 °C on the c-Si wafers for different time durations. As the deposition time increases, the peak amplitude of $<\varepsilon_2>$ at the second transition energy (~ 4.3 eV) deviates more and more from that of the c-Si value. In addition, the onset of absorption shifts to lower energy, indicating the reduction in the optical bandgap of the i_1-a-Si:H layer with an increase in film thickness. Since the amplitude of ε_2 spectra has an inverse relation with the Si–H_2 content in the a-Si:H network [27], we can attribute this amplitude reduction to an enhancement in Si–H_2 content with an increase in the deposition time. The inset of Fig. 7a shows the ε_2 spectra of the same i_1-a-Si:H layers; one can see a gradual increase in the amplitude of the ε_2 peak as the deposition time progresses, which implies that the film density increases with an increase in film thickness.

We employed the Bruggeman effective medium approximation (BEMA) in the spectral ellipsometry analysis

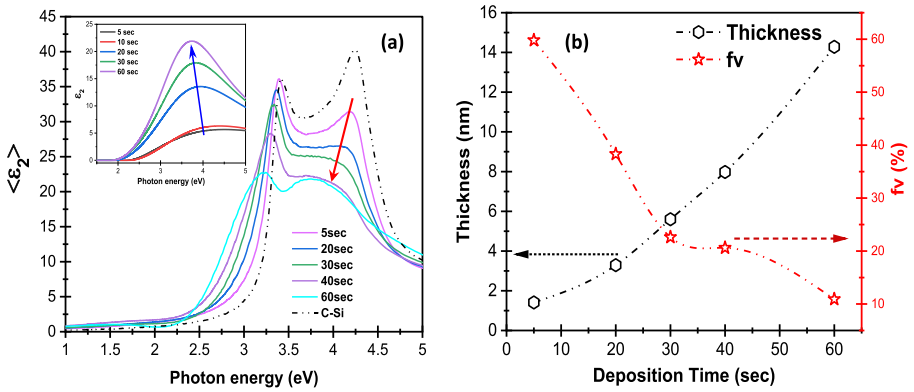

Fig. 7 **a** Variation in the imaginary part of pseudo dielectric function $<\varepsilon_2>$ of i_1-a-Si:H film growth at 150 °C with time, inset of **a** shows the evaluation of ε_2 spectra with time, **b** estimated thickness and a void fraction (f_v) of the i_1-a-Si:H film using ellipsometry analysis with the Bruggeman effective medium approximation model

to estimate the void fraction (f_v) in the i_1-a-Si:H films of varying thicknesses. From Fig. 7b, it is seen that the film's thickness and f_v are inversely related. At the deposition time of ~ 20 s, the effective thickness is found to be ~ 3 nm, and the relative void fraction in the film is estimated to be 40%. As we increase the deposition time, the film's void fraction gradually decreases; hence the compactness of the film is expected to increase. As a result, there is a relatively low possibility of atomic hydrogen diffusion in the film; consequently, the benefit of the stack i-a-Si:H passivation layer may not be effectively realized. However, for the deposition time of ~ 5 s, the relative void fraction is very high (f_v close to 60%); as a result, it contains very high interfacial defects density, and the passivation effect may not be good enough.

3.4 Effect of the i_1-layer thickness in dual-layer on SHJ cell performance

In this subsection, we discuss the effect of different thickness combinations of the LT and HT i-a-Si:H layers in the stack on the passivation and the photovoltaic performance of SHJ solar cells. As the thickness of LT i_1-a-Si:H layer is crucial for the passivation as well as charge carrier transport in the device [5, 6], different thickness combinations of the LT and HT i-a-Si:H layer stack are implemented by maintaining the total i-a-Si:H layer thickness at ~ 10 nm. Table 2 summarizes the passivation results of the cell precursors with p^+-a-Si:H/i_2/i_1/c-Si/i_1/i_2/n^+-a-Si:H structures, the *Suns*-V_{oc}, and illuminated J–V parameters of the complete SHJ cells. We obtained maximum performance parameters when the i_1-a-Si:H thickness is 2 nm; the τ_{eff} of > 2 ms is realized for the cell precursor, the $iV_{oc,}$ pseudo-FF, and pseudo-efficiency being 714 mV and 80.8%, ~ 21.1%, respectively. The cell precursor performance is also reflected in the complete cell, wherein we obtained the highest solar cell J–V parameters with the V_{oc} of 703 mV, FF of 73.5%, and power conversion efficiency of 19.06%. When the thickness of the LT i_1-a-Si:H layer is further increased to 5 nm; the cell precursor results, as well as cell PV parameters, are deteriorated. With a further increase in the LT i_1-a-Si:H layer thickness to 7 nm, the V_{oc}, and FF values dropped to 665 mV and 61.8%, respectively. Hence, 2 nm porous i_1-a-Si:H in the stack is sufficient to realize the full potential of stack passivation, and similar observations have been made in the past [4, 7, 34].

Figure 8 shows the light J–V and pseudo-J–V curves of SHJ cells fabricated with LT-i_1 (2 nm)/HT-i_2 (8 nm) a-Si:H passivating layers stack, inset of the table shows the fill factors and power conversion efficiencies. The significant difference between the FF and p-FF indicates considerable series resistance in a device. This is due to the hindrance in the charge carriers transport from the c-Si to the metal electrodes (within the doped a-Si:H and ITO layers and at different device interfaces). Further optimization of doped a-Si:H layers and other interfaces are required to improve the device's carrier transport. Reducing device series resistance can enhance the fill factor and provide a power conversion efficiency of ≥ 21%, which is under investigation.

The two-step deposition process offers dual advantages: (i) suppresses the chance of epitaxial growth at the a-Si/c-Si interface, (ii) allows the atomic hydrogen penetration into/through the under-dense layer to the a-Si/c-Si interface during the dense i-a-Si:H layer deposition, thereby enhancing the passivation. When the thickness of the LT i_1-a-Si:H layer is reduced to ~ 1 nm, as the combination of (1 + 9) nm stack is used, the precursor sample lifetime and iV_{oc} are good, but at the device, V_{oc}, and FF are mainly limited due to highly disordered nature of interfacial i_1-a-Si:H layer at such a low thickness. It is expected that most of the c-Si surface is

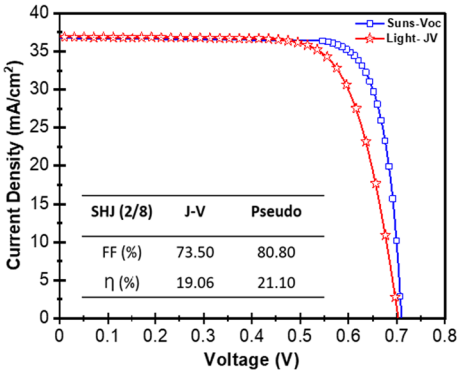

Fig. 8 Light J–V and pseudo-J–V graphs of SHJ cells fabricated using LT-i_1 (2 nm)/HT-i_2 (8 nm) a-Si:H passivating layers stack, inset of the table shows the fill factors and power conversion efficiencies

Table 2 Influence of thickness variation of the two-step passivation i-a-Si:H layer on cell photovoltaic characteristics

Thickness i_1/i_2 (nm)	Cell precursor (i/p/n stack)		*Suns*-V_{oc} results		Device PV parameters				
	τ_{eff} (μs)	iV_{oc} (mV)	pFF (%)	$P\eta$ (%)	J_{sc} (mA/cm^2)	V_{oc} (mV)	FF (%)	η (%)	R_s (Ωcm^2)
1/9	1014	696	77.6	19.4	36.2	682	69.1	17.07	1.72
2/8	2186	714	80.8	21.1	36.8	703	73.5	19.06	1.46
5/5	1037	694	78.6	19.0	35.4	677	66.4	15.94	2.18
7/3	514	675	75.7	18.7	36.9	665	61.8	15.23	2.48

uncovered by the i-a-Si:H layer due to a large void fraction of > 55%, which can be due to inadequate growth conditions. When the thickness of the initial i_1-a-Si:H layer is > 2 nm, it weakens the atomic hydrogen diffusion ability through the i-a-Si:H layer towards the a-Si/c-Si interface, providing inferior passivation, and hence low V_{oc} is observed. Furthermore, V_{oc} is consistently reduced from 703 to 665 mV with the i_1-a-Si:H layer thickness by decreasing the void fraction from 40% to 20%. These observations clearly indicate that an optimum void fraction of around 40% allows penetration of the atomic hydrogen through the porous layer into the amorphous network, so that this atomic H can suppress the interfacial defects and re-passivate the dangling bonds.

4 Conclusions

In this study, we have investigated the temperature-dependent i-a-Si:H layers growth and further on the c-Si surface passivation to minimize the minority carrier recombination by reducing dangling bonds at the interface. The i-a-Si:H layers void fraction and hydrogen bonding environment were analyzed using spectroscopic ellipsometry and FTIR spectroscopy. The void-rich and dense a-Si:H films are formed at low- and high-temperature deposition conditions, respectively. When applied as a single layer, the i-a-Si:H layer deposited at low temperatures showed poor c-Si surface passivation. The low-temperature porous layer deposited at 150 °C ($R^* \sim 0.38$) and high-temperature dense layer at 230 °C ($R^* \sim 0.27$) are applied in the stack together, significantly improving the passivation with an increase in effective minority carrier lifetime. By tuning the i_1-a-Si:H layer thickness (~ 2 nm) with an optimum void fraction of 40% and keeping the total stack thickness of ~ 10 nm, a significant improvement in the effective carriers' lifetime to ~ 2.1 ms led to an enhancement of iV_{oc} of 714 mV.

Acknowledgements Shahnawaz Alam for helping in the transparent conducting oxide layers preparation. The authors would like to acknowledge the financial support from the Department of Science and Technology (DST), Government of India, under the Solar Challenge Award; grant number DST/ETC/CASE/RES/2023/04G, under the Water and Clean Energy area; grant number DST/TMD/CERI/RES/2020/48G of the Technology Mission Division. One of the authors (S.M.) would like to thank DST for providing INSPIRE Faculty award, vide sanction order number DST/INSPIRE/04/2017/000821. The authors acknowledge the Central Research Facility and Nanoscale Research Facility of IIT Delhi for using the FTIR and spectroscopic ellipsometry instruments.

Author contributions AP: conceptualization, methodology, data curation, investigation, formal analysis, writing—original draft, visualization. SB: data curation, investigation, formal analysis. JP: investigation, simulation, writing—review, and editing. SM: methodology, investigation, visualization, project administration, writing—review and editing, funding acquisition. VKK: validation, resources, writing—review and editing, visualization, supervision, funding acquisition.

Data availability All the data set is available from the authors on request.

Declarations

Conflict of interest The authors declare no conflict of interest or competing interest for this work.

References

1. M. Tanaka, M. Taguchi, T. Matsuyama, T. Sawada, S. Tsuda, S. Nakano, H. Hanafusa, Y. Kuwano, Jpn. J. Appl. Phys. **31**, 3518 (1992)
2. D. Adachi, J.L. Hernández, K. Yamamoto, Appl. Phys. Lett. **107**, 233506 (2015)
3. A. Augusto, S.Y. Herasimenka, R.R. King, S.G. Bowden, C. Honsberg, J. Appl. Phys. **121**, 205704 (2017)
4. H. Sai, P.W. Chen, H.J. Hsu, T. Matsui, S. Nunomura, K. Matsubara, J. Appl. Phys. **124**, 103102 (2018)
5. W. Duan, A. Lambertz, K. Bittkau, D. Qiu, K. Qiu, U. Rau, K. Ding, Prog. Photovoltaics Res. Appl. **30**, 384 (2022)
6. C. Luderer, D. Kurt, A. Moldovan, M. Hermle, M. Bivour, Sol. Energy Mater. Sol. Cells **238**, 111412 (2022)
7. A.B. Morales-Vilches, E.C. Wang, T. Henschel, M. Kubicki, A. Cruz, S. Janke, L. Korte, R. Schlatmann, B. Stannowski, Phys. Status Solidi Appl. Mater. Sci. **217**, 1900518 (2020)
8. J. Panigrahi, V.K. Komarala, J. Non. Cryst. Solids **574**, 121166 (2021)
9. J. Ge, Z.P. Ling, J. Wong, R. Stangl, A.G. Aberle, T. Mueller, J. Appl. Phys. **113**, 234310 (2013)
10. A. Descoeudres, L. Barraud, R. Bartlome, G. Choong, S. De Wolf, F. Zicarelli, C. Ballif, Appl. Phys. Lett. **97**, 183505 (2010)
11. A. Soman, A. Antony, Appl. Surf. Sci. **553**, 149551 (2021)
12. T.F. Schulze, L. Korte, B. Rech, Thin Solid Films **520**, 4439 (2012)
13. T. Ruan, M. Qu, J. Wang, Y. He, X. Xu, C. Yu, Y. Zhang, H. Yan, J. Mater. Sci. Mater. Electron. **30**, 13330 (2019)
14. Y. Zhao, P. Procel, A. Smets, L. Mazzarella, C. Han, G. Yang, L. Cao, Z. Yao, A. Weeber, M. Zeman, and O. Isabella, Prog. Photovoltaics Res. Appl. (2022).
15. S. De Wolf, M. Kondo, Appl. Phys. Lett. **90**, 1 (2007)
16. T.F. Schulze, H.N. Beushausen, C. Leendertz, A. Dobrich, B. Rech, L. Korte, Appl. Phys. Lett. **96**, 252102 (2010)
17. J.A. Theil, G. Powell, J. Appl. Phys. **75**, 2652 (1994)
18. R.A. Street, *Hydrogenated amorphous silicon* (Cambridge University Press, 1991)
19. W. Liu, L. Zhang, R. Chen, F. Meng, W. Guo, J. Bao, Z. Liu, J. Appl. Phys. **120**, 175301 (2016)
20. H. Sai, H.J. Hsu, P.W. Chen, P.L. Chen, T. Matsui, Phys. Status Solidi Appl. Mater. Sci. **218**, 2000743 (2021)
21. S. Bhattacharya, A. Pandey, J. Panigrahi, S. Mandal, V.K. Komarala, Appl. Phys. A **129**, 123 (2023)
22. A. Pandey, S. Bhattacharya, J. Panigrahi, S. Mandal, V.K. Komarala, Phys. Status Solidi Appl. Mater. Sci. **219**, 2200183 (2022)
23. M.H. Brodsky, M. Cardona, J.J. Cuomo, Phys. Rev. B **16**, 3556 (1977)
24. A.A. Langford, M.L. Fleet, B.P. Nelson, W.A. Lanford, N. Maley, Phys. Rev. B **45**, 13367 (1992)
25. A.H.M. Smets, W.M.M. Kessels, M.C.M. Van de Sanden, Appl. Phys. Lett. **82**, 1547 (2003)
26. A. Matsuda, Jpn. J. Appl. Phys. **43**, 7909 (2004)

27. S. Kageyama, M. Akagawa, H. Fujiwara, Phys. Rev. B Condens. Matter Mater. Phys. **83**, 195205 (2011)
28. H. Fujiwara, M. Kondo, Appl. Phys. Lett. **90**, 013503 (2007)
29. T.F. Schulze, L. Korte, F. Ruske, B. Rech, Phys. Rev. B Condens. Matter Mater. Phys. **83**, 1 (2011)
30. S. Olibet, E. Vallat-Sauvain, C. Ballif, Phys. Rev. B Condens. Matter Mater. Phys. **76**, 035326 (2007)
31. C. Leendertz, N. Mingirulli, T.F. Schulze, J.P. Kleider, B. Rech, L. Korte, Appl. Phys. Lett. **98**, 202108 (2011)
32. A. Richter, S.W. Glunz, F. Werner, J. Schmidt, A. Cuevas, Phys. Rev. B **86**, 165202 (2012)
33. H. Takato, I. Sakata, R. Shimokawa, Jpn. J. Appl. Phys. Part 2 Lett. **41**, L870 (2002)
34. X. Ru, M. Qu, J. Wang, T. Ruan, M. Yang, F. Peng, W. Long, K. Zheng, H. Yan, X. Xu, Sol. Energy Mater. Sol. Cells **215**, 110643 (2020)